RESEARCH ARTICLE | FEBRUARY 09 2024

Enhanced sensing resolution with microcavity mode oscillation generated by thermal-optic and photorefractive nonlinearity FREE

Xueyi Wang ; Jiangwei Wu ; Chengyu Chen ; Tingge Yuan ; Yuping Chen ; Xianfeng Chen

Appl. Phys. Lett. 124, 061108 (2024)
https://doi.org/10.1063/5.0188236

Enhanced sensing resolution with microcavity mode oscillation generated by thermal-optic and photorefractive nonlinearity

Cite as: Appl. Phys. Lett. **124**, 061108 (2024); doi: 10.1063/5.0188236
Submitted: 20 November 2023 · Accepted: 20 January 2024 ·
Published Online: 9 February 2024

Xueyi Wang,[1] Jiangwei Wu,[1] Chengyu Chen,[1] Tingge Yuan,[1] Yuping Chen,[1,2,a)] and Xianfeng Chen[1,3,4]

AFFILIATIONS

[1]State Key Laboratory of Advanced Optical Communication Systems and Networks, School of Physics and Astronomy, Shanghai Jiao Tong University, No. 800 Dongchuan Road, Shanghai 200240, China
[2]School of Physics, Ningxia University, 217 North Wencui Street, Yinchuan 750021, China
[3]Shanghai Research Center for Quantum Sciences, Shanghai 201315, China
[4]Collaborative Innovation Center of Light Manipulations and Applications, Shandong Normal University, No. 1, University Road, Jinan 250358, China

[a)]Author to whom correspondence should be addressed: ypchen@sjtu.edu.cn

ABSTRACT

Optical microcavity has proven its potential for unlabeled sensing. Here, we propose and demonstrate in a lithium niobate on insulator microcavity an enhanced sensing approach enabled by the nonlinear mode oscillation generated by the competition between thermal-optic and photorefractive effect, which breaks the intrinsic limitation in wavelength resolution set by the cavity's optical quality factor. It allows us to perform precise measurements of the mode shifting introduced by a nanoscale scatterer with a signal to noise ratio of 13.1 dB and paves a distinctive way to improve resonance shift resolution in widely studied microcavity sensors with a platform of great integration capability.

The utilization of optical microcavity sensors has promised unprecedented high sensitivity with its high Q factor (quality factor) and small mode volume,[1–3] whose mechanism relies on the strong light–matter interference enabled by the light constantly circulating inside the cavity,[3] and when a particle binds to the cavity's equator, it disturbs the original resonance with a shift[4–8] $\delta\lambda$, a splitting[9,10] or broadening.[11] However, the most adapted mode shifting method relies critically on the cavity's Q factor.[12] Only with a Q factor as high as 10^8 can it reach the resolution of tenth fm[13] yet still not enough for protein detection for bio-sensing.[14] Brand new principles have been introduced into microcavity systems to overcome such limitations, including active lasing[15] that significantly increased light–matter interaction, and nonlinear process of mode[16–18] or opto-mechanical coupling[19] that enhanced sensing resolution by magnitudes.

Meanwhile stable nonlinear mode oscillation (NMO) has been observed in high-quality microcavities resulting from a variety of nonlinear effects, such as the competition between thermal-optic and thermal expansion,[20] free carrier generation,[21] mechanical deformation,[22] Kerr effect,[23] and Brillouin scattering.[24] Specifically, in lithium niobate on insulator (LNOI) microcavities, its outstanding electro-optical properties[25] allow the unique competition of thermal-optic and photorefractive effect[26] generating a very robust NMO even with a compromised Q factor, creating a NMO frequency reacting dependently to the laser detuning $\delta\lambda_0 = \lambda_L - \lambda_0$.[20–22,26] The wavelength shift $\delta\lambda$ caused by the scatterer would then appear in the frequency change of NMO $\delta f = \frac{df}{d(\delta\lambda_0)}\delta\lambda$ read from the transmission spectrum of a fixed pump laser as shown in Figs. 1(a)–1(c). The resolution limit for mode shifting $(\delta\lambda)_{min} = \sigma_f / \frac{df}{d(\delta\lambda_0)}$ is now only up to the variation σ_f of NMO, avoiding variations caused by the Q factor and spectral resolution of the setup.

Herein, we utilized the NMO of a Z-cut LNOI microcavity to demonstrate its sensing enhancement with the experimental setup as Fig. 1(d). The chip was first milled by a focused ion beam (FIB, ZEISS Auriga) and then immersed into a buffered oxide etching solution to build a microdisk with a diameter of 16 μm, a thickness of 300 nm, and a stull diameter of around 10 μm. We use an FG (function generator) to piezoelectrically control the TL (tunable laser), which is injected into a VOA (variable optical attenuator) to accurately control laser output power. A circulator allows us to read transmission and

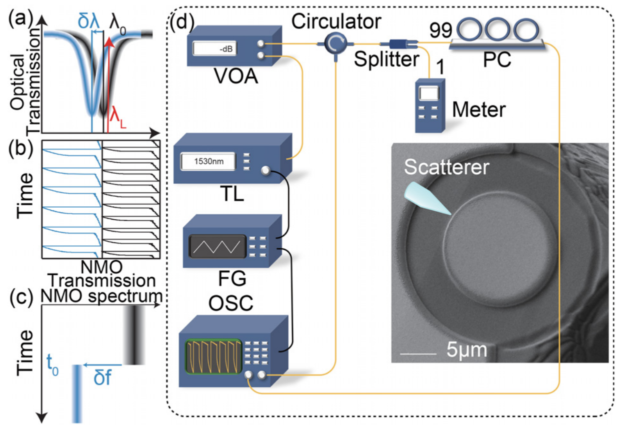

FIG. 1. Schematic diagrams of the NMO sensing process: (a) under a fixed laser input the cavity mode could (b) generate a NMO f highly sensitive to the laser's detuning. (c) Thus, the mode shifting is observed in the δf, which is acquired from the square-wave Fourier transformation of the oscillation transmission spectrum. (d) Experimental setup, including a SEM (scanning electron microscope) image of the microdisk. The scatterer is a SiO_2 tapered single mode fiber tip with a radius of around 150 nm. VOA (variable optical attenuator), TL (tunable laser), FG (function generator), OSC (oscilloscope), and PC (polarization controller).

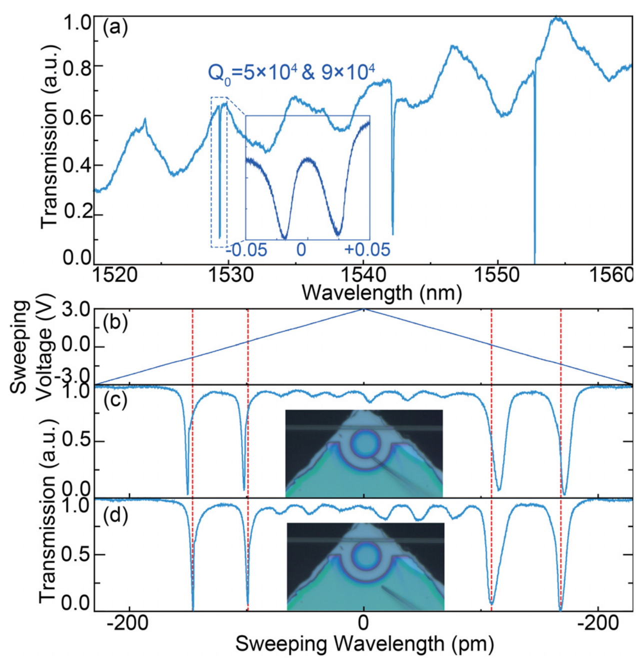

FIG. 2. (a) Transmission spectrum of the microdisk, and inset is the mode at 1529.5 nm utilized by this work and Q factors acquired by applying Lorentzian fitting to each dip, respectively. (b) Output voltage of the FG to piezoelectrically drive the laser scan across a 30 GHz frequency range. Scanned transmission spectrum (c) with and (d) without a scatterer under an input power of $P_{in} = 71.4\,\mu$W, and the insets are micrographic photos of the experiment.

reflection spectra simultaneously to accurately adjust the coupling coefficient of the tapered fiber. The transmission spectrum of the cavity is as Fig. 2(a), which has a split resonance mode at 1529.5 nm whose loaded Q factors are 50k and 90k that lead to linewidth of 30.6 and 17 pm. It has theoretical minimum detectable mode shifts $(\delta\lambda)_{min}$[12] of 3.63 and 3.21 pm, respectively. To estimate the shift caused by the scatterer as in Figs. 2(b)–2(d) we scan back and forth with piezoelectric control. The spectrum shows a mode shift of −3.53 and −6.44 pm without significant mode broadening when the taper is attached. The sharp asymmetric line shape reveals the generation of photorefraction,[27] for it shifts the mode blue as the laser is scanning toward a longer wavelength.

To verify the NMO sensing scheme suggested above, we then keep the laser scanning at 0.1 nm/s to leave sufficient amount of time generating NMO at every detuned wavelength, which causes very strong broadening as shown in Fig. 3(a). Then, we stop the laser at different detuned wavelengths during scanning and mark the bluest detuned wavelength that generates stable oscillation as 0 pm, and a series of oscillation is generated at detuned wavelength 0–120 pm as the case (i) to (iv) in Fig. 3(b) with an input laser power of $P_{in} = 792.5\,\mu$W. It can be seen clearly that the NMO frequency $f = 1/t_1$ would first increase and then decrease as the laser is less blue detuned, while its MSR (mark–space ratio) $= \frac{t_1 - t_0}{t_0}$ increases along the way; the following is a detailed theoretical explanation.

The nonlinear dynamics in LNOI microcavity can be described as[26,28–30]

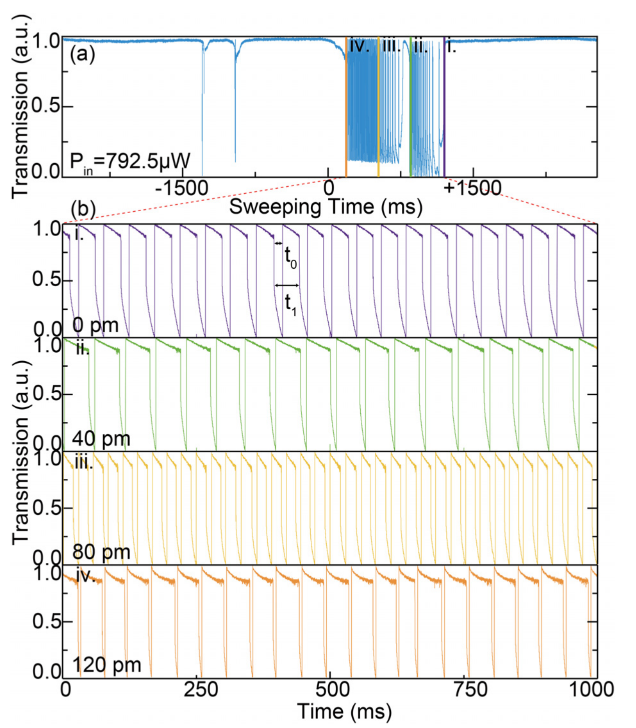

FIG. 3. (a) Laser-scanned cavity transmission spectrum with a back and forward scanning rate of 0.1 nm/s. (b) The nonlinear oscillation spectrum when the laser is fixed at certain detuned wavelength [(i)–(iv) from (a)], at an input optical power of $P_{in} = 792.5\,\mu$W.

$$\frac{da}{dt} = (i\delta\omega_0 - \Gamma_t)a - ig_T\Delta Ta - ig_E E_{sc}a + i\sqrt{\Gamma_e}A, \quad (1)$$

where the first and last parts describe the cavity resonance before NMO is yet generated $\delta\omega_0 = \omega_L - \omega_0$ and Γ_t and Γ_e are the total and external loss of the cavity with input laser amplitude A. The second and third terms reflect the frequency shift caused by photothermal coupling $g_T = -\omega_0\left(\frac{1}{n_e}\frac{dn_e}{dT} + \Lambda^{X,Y}\right)$ and electro-optic coupling $g_E = \frac{d\omega_0}{dE} \approx n_e^2\omega_0\gamma_{22}/2$, and γ_{22} is the LN electro-optic coefficient. In a Z-cut LNOI chip, there is a positive thermo-optic coefficient[31] $\frac{dn_e}{dT} \approx 3.34 \times 10^{-5}$/K and a positive thermo-expansion coefficient[32] as well $\Lambda^{X,Y} = 0.748 \times 10^{-5}$/K. The temperature and space-charge electric field variation could both be described in two parts separately for its relaxation and generation[26,28–30] process, as $\frac{d\Delta T}{dt} = -\Gamma_T\Delta T + \eta_T|a|^2$ and $\frac{dE_{sc}}{dt} = -\Gamma_E E_{sc} + \eta_E|a|^2$, in which Γ_T is dependent on the thermal properties of the material and the geometrical size of the device. The heating coefficient η_T is determined by the optical absorption and heat conversion.[29] The dynamics of the space-charge electric field works in a similar way as the carriers are also excited by optical absorption.[26]

With the laser originally blue detuned at $\delta\omega_0$, the thermal-optic effect would first cause a rapid red shift $\delta\omega_T = g_T\eta_T|a(\delta\omega_0)|^2$, pushing the laser to its red detuned side $\delta\omega_1 = \delta\omega_0 + \delta\omega_T$. Then, the photorefractive effect starts to accumulate slowly pulling the cavity mode blue until the laser is on resonance where $\delta\omega_2 = \delta\omega_1 - \delta\omega_E = 0$, causing a "space" span $t_0 = \int_{\omega_0+\delta\omega_1}^{\omega_0} \frac{d\omega}{g_E\eta_E|a(\omega)|^2}$ leaving electric field at $E_{sc}(t_0) = g_E\eta_E\int_{\omega_0+\delta\omega_1}^{\omega_0}|a(\omega)|^2 d\omega$ as it accumulates over time. At this point, any more detuning causes $\delta\omega_T$ to relax also rapidly, and the laser input is now further blue detuned $\delta\omega_3 = \delta\omega_0 - \delta\omega_E$. The laser power hardly couples into the cavity at this point so E_{sc} also begins to wear out and slowly red shifting the cavity modes toward where the NMO originally started; consequently, the mark period lasts for $t_1 - t_0 = \frac{\ln E_{sc}(t_0)}{\Gamma_E}$. The generation and relaxation time of thermo-refraction is generally much faster than photovoltaic current, leading to a sharp falling and rising edge in the NMO spectrum shown in Fig. 3(b). As a result, the NMO has a frequency and MSR highly sensitive to the laser detuning and can be only generated when the laser locates within the cavity mode.

After the same measurement of Fig. 3 is performed at different P_{in}, we clearly captured the dependence of oscillation properties on P_{in} and $\delta\lambda_0$ as shown in Figs. 4(a) and 4(b), which is acquired from the transmission spectrum of 1 s, and the error bar indicates the variation σ_f of f and MSR within the sampling span. The frequency obviously drops with a higher P_{in}, for it causes larger thermal-optical red shift and thus prolongs the competition time. Both frequency and MSR agree with previous theoretical analysis very well, and the slope of the fitted curve $\frac{df}{d(\delta\lambda_0)}$ shows how NMO frequency reacts to laser detuning. Only at lower input power, the oscillation is unstable at the edges of both cavity resonance modes so we choose to operate the sensor with P_m and P_h at wavelengths where stable NMO is generated. First, we make sure the oscillation is robust over time as in Figs. 4(c) and 4(d), and the oscillation frequency is acquired with a sampling time of 1 s in every other 10 s within the sampling span, from which we could tell that even though the laser instability does cause a few fluctuations that still locate within the error bar, both oscillation frequency and MSR are stabilized after at most 40 s, and we only perform sensing after this.

Next, we add the scatterer to the cavity as previously in Fig. 2, and only at this time, the laser is fixed to generate a stable oscillation. It enables us to acquire the mode shifting now from the NMO frequency domain as in Fig. 4(g) and MSR domain in Fig. 4(h). Here, we mark the maximum shift as $\delta f_m(\delta MSR_m)$ after the taper is attached and the shift between the steady oscillation as $\delta f_s(\delta MSR_s)$ before scattering

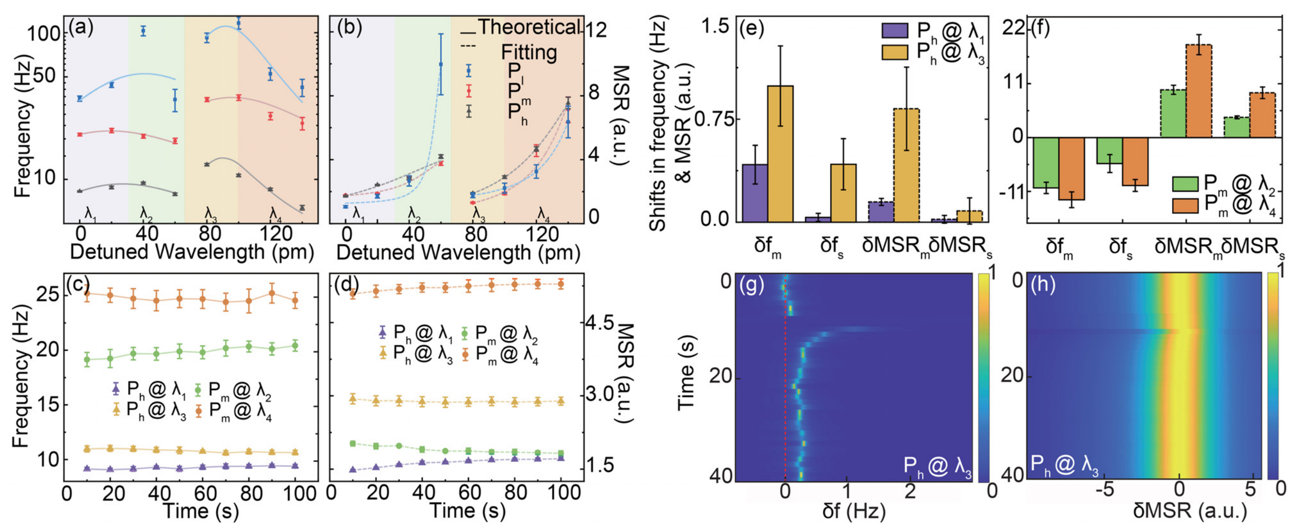

FIG. 4. (a) and (b) Nonlinear oscillation properties at different input power and detuned wavelength. Here, $P_l = 490.8\ \mu$W, $P_m = 792.5\ \mu$W, and $P_h = 1285\ \mu$W. The four sections of λ_i, $i = 1, 2, 3, 4$, are roughly divided by the sign of $\frac{df}{d(\delta\lambda_0)}$. Stability of NMO frequency (c) and MSR (d) generated at different P_{in} and detuned wavelength at a time span of 100 s. Shifts in NMO frequency (e) and MSR (f) when interfered by the tapered fiber. The oscillation is generated at the same P_{in} and detuned frequency that have been previously proven robust. Each measurement is repeated ten times for every oscillation status. (g) and (h) The oscillation frequency and MSR domain for each measurement in 40 s.

and after the taper is removed for the coupling condition could be disturbed by the movements. $\delta f = \delta f_m - \delta f_s$ would fully represent the generation of mode shift and its relaxation. Every time before another test, we would switch the laser back to scanning and slightly adjust the coupling fiber to make sure the reflection spectrum is of the same amplitude as before, and in this way, we could decrease the fluctuation in coupling loss to its minimum. After a repetition of ten times at each P_{in} and $\delta\lambda$, the test appears with a similar shift that distributes as Figs. 4(e) and 4(f). With $\delta f / \frac{df}{d(\delta\lambda_0)} = \delta\lambda$, the shifting caused by the scatterer is then calculated to be -8.76 ± 3.0, -10.4 ± 3.0, -9.5 ± 2.0, and -10.31 ± 1.3 pm for the four groups of attempts at $P_h@\lambda_1$, $P_h@\lambda_3$, $P_m@\lambda_2$, and $P_m@\lambda_4$, respectively, with $\frac{df}{d(\delta\lambda_0)} = 46.8$, 55.4, -306, and -320 Hz/nm. The direction of $\delta\lambda$ is in the same time told from the decrease in MSR. The results fit well with the estimation done in Fig. 2 with a signal to noise ratio of 13.1 dB. A maximum resolution of 1.63 pm can be achieved in theory from the variation σ_f shown in Figs. 4(a) and 4(b), which can be further improved with a more stable experimental setup.

In this paper, a microcavity NMO sensor is demonstrated, and its fundamental nonlinear dynamics between thermal-optic and photorefractive effect in LNOI is also analyzed and tested in detail, revealing the connection between nonlinear oscillation properties and input pump laser power and detuning. Despite its natural liability with a moderate Q factor, the nonlinear oscillation microcavity sensor offered accurate and stable feedback for the mode shift caused by the nanoscale scatterer and a minimum resolution overcoming the intrinsic limitation set by optical Q factor. This proves its giant potential for unlabeled sensing of biomolecule, minor refractive index change, environmental monitoring, and many other microcavity sensing platforms that rely on a Q factor for better sensitivity. However, this approach does require a higher pump power and a non-instant response time, which can be improved with better fabrication technique. Here, we have confined our discussions within the LNOI platform, and we believe this method can be demonstrated with other cavity-based sensors utilizing abundant nonlinear dynamics yet discovered[20–24] with great integration capability.

This work was supported by the National Natural Science Foundation of China (Grant No. 12134009), the National Key R&D Program of China (Grant No. 2019YFB2203501), and SJTU No. 21X010200828.

AUTHOR DECLARATIONS

Conflict of Interest

The authors have no conflicts to disclose.

Author Contributions

Xueyi Wang: Conceptualization (lead); Formal analysis (lead); Investigation (lead); Methodology (lead); Visualization (lead); Writing – original draft (lead); Writing – review & editing (lead). **Jiangwei Wu:** Conceptualization (equal); Investigation (equal); Methodology (equal); Writing – review & editing (equal). **Chengyu Chen:** Investigation (equal); Writing – review & editing (equal). **Tingge Yuan:** Conceptualization (equal); Writing – review & editing (equal). **Yuping Chen:** Funding acquisition (lead); Supervision (lead). **Xianfeng Chen:** Supervision (equal).

DATA AVAILABILITY

The data that support the findings of this study are available from the corresponding author upon reasonable request.

REFERENCES

[1] A. M. Armani, R. P. Kulkarni, S. E. Fraser, R. C. Flagan, and K. J. Vahala, "Label-free, single-molecule detection with optical microcavities," Science **317**, 783–787 (2007).
[2] F. Vollmer and L. Yang, "Review label-free detection with high-Q microcavities: A review of biosensing mechanisms for integrated devices," Nanophotonics **1**, 267–291 (2012).
[3] Y. Zhi, X.-C. Yu, Q. Gong, L. Yang, and Y.-F. Xiao, "Single nanoparticle detection using optical microcavities," Adv. Mater. **29**, 1604920 (2017).
[4] F. Vollmer, D. Braun, A. Libchaber, M. Khoshsima, I. Teraoka, and S. Arnold, "Protein detection by optical shift of a resonant microcavity," Appl. Phys. Lett. **80**, 4057–4059 (2002).
[5] O. Gaathon, J. Culic-Viskota, M. Mihnev, I. Teraoka, and S. Arnold, "Enhancing sensitivity of a whispering gallery mode biosensor by subwavelength confinement," Appl. Phys. Lett. **89**, 223901 (2006).
[6] C.-H. Dong, L. He, Y.-F. Xiao, V. R. Gaddam, S. K. Ozdemir, Z.-F. Han, G.-C. Guo, and L. Yang, "Fabrication of high-Q polydimethylsiloxane optical microspheres for thermal sensing," Appl. Phys. Lett. **94**, 231119 (2009).
[7] S. I. Shopova, R. Rajmangal, S. Holler, and S. Arnold, "Plasmonic enhancement of a whispering-gallery-mode biosensor for single nanoparticle detection," Appl. Phys. Lett. **98**, 243104 (2011).
[8] V. R. Dantham, S. Holler, V. Kolchenko, Z. Wan, and S. Arnold, "Taking whispering gallery-mode single virus detection and sizing to the limit," Appl. Phys. Lett. **101**, 043704 (2012).
[9] A. Mazzei, S. Götzinger, L. de S. Menezes, G. Zumofen, O. Benson, and V. Sandoghdar, "Controlled coupling of counterpropagating whispering-gallery modes by a single rayleigh scatterer: A classical problem in a quantum optical light," Phys. Rev. Lett. **99**, 173603 (2007).
[10] W. Kim, a K. Özdemir, J. Zhu, L. He, and L. Yang, "Demonstration of mode splitting in an optical microcavity in aqueous environment," Appl. Phys. Lett. **97**, 071111 (2010).
[11] L. Shao, X.-F. Jiang, X.-C. Yu, B.-B. Li, W. R. Clements, F. Vollmer, W. Wang, Y.-F. Xiao, and Q. Gong, "Detection of single nanoparticles and lentiviruses using microcavity resonance broadening," Adv. Mater. **25**, 5616–5620 (2013).
[12] I. M. White and X. Fan, "On the performance quantification of resonant refractive index sensors," Opt. Express **16**, 1020–1028 (2008).
[13] T. Lu, H. Lee, T. Chen, S. Herchak, J.-H. Kim, S. E. Fraser, R. C. Flagan, and K. Vahala, "High sensitivity nanoparticle detection using optical microcavities," Proc. Natl. Acad. Sci. U. S. A. **108**, 5976–5979 (2011).
[14] F. Vollmer and S. Arnold, "Whispering-gallery-mode biosensing: Label-free detection down to single molecules," Nat. Methods **5**, 591–596 (2008).
[15] L. He, Ş. K. Özdemir, J. Zhu, W. Kim, and L. Yang, "Detecting single viruses and nanoparticles using whispering gallery microlasers," Nat. Nanotechnol. **6**, 428–432 (2011).
[16] B.-B. Li, Y.-F. Xiao, C.-L. Zou, Y.-C. Liu, X.-F. Jiang, Y.-L. Chen, Y. Li, and Q. Gong, "Experimental observation of Fano resonance in a single whispering-gallery microresonator," Appl. Phys. Lett. **98**, 021116 (2011).
[17] S. Fan, "Sharp asymmetric line shapes in side-coupled waveguide-cavity systems," Appl. Phys. Lett. **80**, 908–910 (2002).
[18] W. Chen, Ş. Kaya Özdemir, G. Zhao, J. Wiersig, and L. Yang, "Exceptional points enhance sensing in an optical microcavity," Nature **548**, 192–196 (2017).
[19] W. Yu, W. C. Jiang, Q. Lin, and T. Lu, "Cavity optomechanical spring sensing of single molecules," Nat. Commun. **7**, 12311 (2016).
[20] W. Weng, J. D. Anstie, P. Abbott, B. Fan, T. M. Stace, and A. N. Luiten, "Stabilization of a dynamically unstable opto-thermo-mechanical oscillator," Phys. Rev. A **91**, 063801 (2015).

[21]J. Yang, T. Gu, J. Zheng, M. Yu, G.-Q. Lo, D.-L. Kwong, and C. Wei Wong, "Radio frequency regenerative oscillations in monolithic high-Q/V heterostructured photonic crystal cavities," Appl. Phys. Lett. **104**, 061104 (2014).
[22]H. Itobe, Y. Nakagawa, Y. Mizumoto, H. Kangawa, Y. Kakinuma, and T. Tanabe, "Bi-material crystalline whispering gallery mode microcavity structure for thermo-opto-mechanical stabilization," AIP Adv. **6**, 055116 (2016).
[23]C. Schmidt, A. Chipouline, T. Pertsch, A. Tünnermann, O. Egorov, F. Lederer, and L. Deych, "Nonlinear thermal effects in optical microspheres at different wavelength sweeping speeds," Opt. Express **16**, 6285–6301 (2008).
[24]Y. Qin, S. Ding, S. Lei, J. Liu, Y. Bai, M. Zhang, Y. Li, J. Wen, X. Jiang, and M. Xiao, "Self-pulsations in a microcavity brillouin laser," Opt. Lett. **47**, 421–424 (2022).
[25]R. Weis and T. Gaylord, "Lithium niobate: Summary of physical properties and crystal structure," Appl. Phys. A **37**, 191–203 (1985).
[26]X. Sun, H. Liang, R. Luo, W. C. Jiang, X.-C. Zhang, and Q. Lin, "Nonlinear optical oscillation dynamics in high-Q lithium niobate microresonators," Opt. Express **25**, 13504–13516 (2017).
[27]A. A. Savchenkov, A. B. Matsko, D. Strekalov, V. S. Ilchenko, and L. Maleki, "Enhancement of photorefraction in whispering gallery mode resonators," Phys. Rev. B **74**, 245119 (2006).
[28]T. Carmon, L. Yang, and K. J. Vahala, "Dynamical thermal behavior and thermal self-stability of microcavities," Opt. Express **12**, 4742–4750 (2004).
[29]A. E. Fomin, M. L. Gorodetsky, I. S. Grudinin, and V. S. Ilchenko, "Nonstationary nonlinear effects in optical microspheres," J. Opt. Soc. Am. B **22**, 459–465 (2005).
[30]X. Sun, R. Luo, X.-C. Zhang, and Q. Lin, "Squeezing the fundamental temperature fluctuations of a high-Q microresonator," Phys. Rev. A **95**, 023822 (2017).
[31]L. Moretti, M. Iodice, F. G. Della Corte, and I. Rendina, "Temperature dependence of the thermo-optic coefficient of lithium niobate, from 300 to 515 K in the visible and infrared regions," J. Appl. Phys. **98**, 036101 (2005).
[32]Y. S. Kim and R. T. Smith, "Thermal expansion of lithium tantalate and lithium niobate single crystals," J. Appl. Phys. **40**, 4637–4641 (2003).